A Novel Scalable Digital Data Acquisition System for Industrial Condition Monitoring

A novel scalable digital data acquisition system for industrial condition monitoring

Andrea Toscani, Fabio Immovilli, *Senior Member, IEEE*, Daniel Pinardi, and Luca Cattani

***Abstract*—This paper introduces a novel data acquisition (DAQ) system aimed at condition monitoring of complex industrial machinery and plants. Current commercial solutions can be divided into two groups: high resolution and data rate rack systems or distributed systems usually at the price of lower performance. The proposed solution aims at filling this gap. It relies on a daisy-chain digital bus architecture, featuring a main node and a series of subordinate nodes, which have been designed to collect data from both analog and digital transducers. It follows that the system is highly scalable and easily reconfigurable: the number and the type of transducers, ranging from low-cost Micro Electro-mechanical Systems (MEMS) to high quality piezoelectric sensors, can be optimized to match each specific measurement requirements, even after the installation of the system. The proposed technology supports up to 32 channels at 48 kS/s, and guarantees the perfect synchronization of all signals regardless of the transducer type and its position along the bus, allowing to perform advanced data analysis. The system performance is at first evaluated with laboratory tests, then in the scenario of condition monitoring of rolling bearing faults, demonstrating good sensitivity and coherence between different accelerometer types.**

***Index Terms*—analog IEPE accelerometer, bearing fault detection, data acquisition system, digital bus, industrial condition monitoring, MEMS accelerometer, scalable architecture, structural health monitoring.**

I. Nomenclature

fs	Sampling frequency.
n_{FFT}	Number of frequency bins.
f	Mains frequency.
F_r	Rotor mechanical frequency.
F_{inner}	Inner ring fault frequency.
F_{outer}	Outer ring fault frequency.
F_{cage}	Cage fault frequency.
F_{ball}	Ball (rolling element) fault frequency.
D_c	Pitch diameter.
D_b	Ball (rolling element) diameter.
n	Number of rolling elements.
β	Contact angle.
a	Acceleration.

Subscripts

cal	Calibrator.
ref	Reference value.
rms	Root mean square.

Manuscript received December 29, 2022; revised April 27, 2023; revised June 15, 2023; accepted July 22, 2023. This work was supported by ASK Industries S.p.A.

Funder: Project funded under the National Recovery and Resilience Plan (NRRP), Mission 4 Component 2 Investment 1.5 - Call for tender No. 3277 of 30/12/2021 of Italian Ministry of University and Research funded by the European Union - NextGenerationEU Award Number: Project code ECS-00000033, Concession Decree No. 1052 of 23/06/2022 adopted by the Italian Ministry of University and Research, CUP B33D21019790006, Ecosystem For Sustainable Transition of Emilia-Romagna (ECOSISTER).

(Corresponding author: Andrea Toscani. Phone: +39 0521 906007)

A. Toscani and D. Pinardi are with the Department of Engineering and Architecture, University of Parma, Parma, 43124, Italy (e-mail: andrea.toscani@unipr.it; daniel.pinardi@unipr.it).

F. Immovilli is with the Department of Sciences and Methods for Engineering, University of Modena and Reggio Emilia, Reggio Emilia, 42122, Italy (e-mail: fabio.immovilli@unimore.it).

L. Cattani is with ASK Industries S.p.A., Reggio Emilia, 42124, Italy (e-mail: luca.cattani@askgroup.global).

II. Introduction

FAULT detection and diagnosis in rotating machinery has been the subject of an extensive research in the last decades with the goal of optimizing maintenance and cost savings through better information-based decision making.

A. Literature Review and Motivation

Condition and vibration monitoring systems can assist in keeping industrial production plants running by detecting potential failures in a timely manner. Incipient faults of rotating equipment in noisy environment can easily go undetected until a major damage or catastrophic failure occurs. Fault detection at the early stage via noninvasive fault diagnosis is preferred, allowing for scheduled maintenance and minimizing system downtime.

Many scientific articles concern the problem of general condition monitoring (CM) of electric machines [1] and fault occurrence distribution among the machine components [2]. Focusing on the mechanical faults, bearing faults are one of the most common failure mode in industrial machinery also according to manufacturers' statistics, [3], where bearing related faults account for more than 50% of motor failures. Bearing faults that are not timely detected may result in: reduced performance, degraded efficiency, overheating and malfunctions, up to catastrophic failure of the driven machinery [4], [5]. Fault diagnosis methods based on the analysis of vibration signals are well established and have proven their effectiveness in many situations, [6]. By processing the raw data, fault conditions can be identified and, ideally, major breakdowns

prevented before they occur. Suitable signal processing techniques are required to efficiently extract and isolate the fault signatures from raw signal, since fault signatures at incipient stage feature a very small amplitude that is usually buried in noise and thus can lead to false positive detection [7]. When considering the vibration signal, the two most commonly used indicators are the Root Mean Square value (RMS) of the vibration velocity [8] and the kurtosis [9]. More refined statistical approach and feature extraction algorithms are also employed, especially when fault classification is of interest [10].

Very simple and low-cost CM was traditionally limited to routine inspections since the diagnosis equipment is expensive and requires dedicated transducers to be installed on the monitored machinery. More sophisticated and expensive vibration CM can be employed as an on-line fault detection tool: under these circumstances the CM systems rely on data collected via automation systems or even dedicated sensor networks to constantly monitor the operating condition of the plant, [11].

Structural Health Monitoring (SHM) techniques [12]–[15] in the field of maintenance of civil structures, industrial plants, and machines, usually use analog systems based on a star topology for the transducers' data acquisition (DAQ) net. In modal analysis techniques, a perfect temporal alignment in the measured signals is mandatory, and therefore a wired link from sensors to a centralized acquisition system is still preferred with respect to a wireless solution [16], even at the price of redundant cabling and installation rising costs. Furthermore, long analog cables suffer from signal degradation, which is particularly present in highly electromagnetic disturbed environments, such as factories and industrial plants [17]. Similar considerations apply in the case of CM of large industrial machinery in production plants, [18] and also in case of renewable energy sources installations such as wind turbines, [19], [20] or hydroelectric plants, [19]. Whenever the CM algorithms are based on cross-correlation of vibration signals taken at different positions of the machinery, as in the case of large gearboxes, perfect temporal alignment of the different channels is mandatory. The latter requirement favors, again, wired networks over wireless ones, [21].

Despite piezoelectric transducers have been widely employed in the last decades [22], as they provide high quality signal with a low self-noise [23], a trend toward MEMS transducers is currently observed [24], as the performance of the latter is constantly improving [25], [26]. Although a sensitivity lower than piezoelectric transducers, digital MEMS solutions are more and more preferred due to their low cost and immunity to electromagnetic noise.

Vibration analysis is the preferred method for fault detection and CM of rotating equipment and structures in general. The typical setup comprises acceleration transducers, a digital recorder and post-processing algorithms for real-time or off-line analysis of the recorded signals.

Most of the systems available on the market have a standardized, modular construction, Tab. I. Transducers are usually piezoelectric with an integrated charge amplifier and are connected to a dedicated multi channel DAQ card or module housed in a rack or frame. A number of racks can be connected in a monitoring network, but since the Analog-to-Digital converter (ADC) is usually separated from the transducers, multiple channels must be individually connected to the respective DAQ platform using dedicated wiring. When dealing with large, complex machinery or when monitoring large structures, this translates into complex wiring looms that are expensive, difficult to lay out, and susceptible to electromagnetic noise pick-up. The few examples of stand-alone networked vibration monitoring nodes are characterized by a significantly lower performance. As it can be seen, there is a significant performance gap between the centralized DAQ platforms and the networking sensor nodes. Modular rack systems are characterized by high resolution, fast sampling frequency, and excellent time integrity of the acquired data but they require a complex analog wiring between the analog transducers and the centralized DAQ system. Network nodes, on the other hand, simplify the wiring and improve electromagnetic noise immunity, at the expense of bandwidth, resolution, and inferior time integrity of the acquired data.

TABLE I
OVERVIEW OF COMMERCIAL VIBRATION MONITORING SYSTEMS

Company name	**Model name**	**Channels [n]**	**Rate [kS/s]**	**Resolution [bits]**
Siemens	Scadas V8 card	8	204.8	24
NI	NI-9234 module	4	51.2	24
Beckhoff	EL3632 module	2	50	16
Beckhoff	EP3752 2x 3-axis	6	5	10

The proposed solution aims to overcome these limitations by providing a platform that, while retaining the modular approach, is inherently digital, since the ADC is incorporated in each acquisition node, also providing a flexibility in selecting the transducer, that can be a piezoelectric or MEMS accelerometer. The main advantages of the proposed solution, that will be detailed in the following section, are: scalability, ease of reconfiguration, flexibility of transducers choices, and fully digital two-wire bus connection to simplify wiring on the field and increase electromagnetic noise immunity with respect to an analog wiring.

B. Contribution and paper organization

In this paper, it is described an innovative DAQ system, shown in Fig. 1 a), based on the Automotive Audio Bus (A^2B) [27], a protocol developed by Analog Devices for distributing audio signals inside vehicles, with the aim of reducing the number, the weight, and the cost of the cabling. In SHM and CM applications, it solves all the previously mentioned problems. A^2B allows connecting multiple nodes in a daisy-chain configuration, therefore overcoming the cabling redundancy of a star topology. The cost of the cabling is considerably reduced too, since A^2B makes use of an Unshielded Twisted Pair (UTP) wire, which carries both the data and the phantom power supply. The main innovations of the proposed solution are the simplification of the sensor net topology and the flexibility of the utilization. In fact, both analog and digital nodes can co-exist on the same A^2B network, thus allowing for a hybrid architecture, whose schematic is depicted in Fig. 1 b). For this

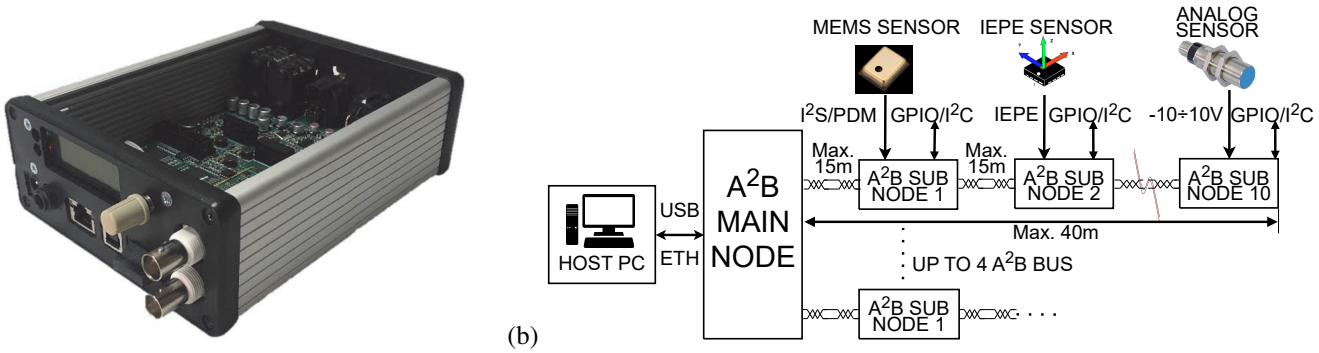

(a) (b)

Fig. 1. A^{2}B Digital data acquisition system: a) Main Node prototype b) Block diagram of the sensor network.

work, a full-digital node has been designed, integrating a tri-axial digital MEMS accelerometer. A hybrid node has been designed too, integrating the ADC, thus making it possible to acquire piezoelectric transducers. It allows for a local Analog-to-Digital conversion of the signal, thus preserving the Signal-to-Noise Ratio (S/N), without increasing the complexity and the length of the cabling. The solution is also flexible, since it allows employing at the same time low-cost MEMS and top-quality piezoelectric transducers, enabling the choice of the optimal one depending on the components to be monitored.

The paper is organized as follows: Section III introduces the proposed DAQ architecture, along with its advantages and drawbacks. Section IV presents the experimental comparison between the proposed hybrid architecture DAQ against a commercial DAQ, when piezoelectric transducers are employed. Section V presents a bearing fault detection case study, where the proposed hybrid architecture DAQ is fitted with both piezoelectric as well as MEMS accelerometers in order to assess the respective performance. The experimental results obtained in the previous tests are summarized in VI. Finally, the Conclusion section is dedicated to a discussion of the results and concluding remarks.

III. System overview

The proposed DAQ system is based on the A^{2}B technology, a digital audio bus developed by Analog Devices. Although A^{2}B was designed for automotive applications, it offers several advantages when employed in the industrial field to acquire signals from multiple sensors [28]. In particular, an A^{2}B bus allows to transport sensors data, General Purpose Input/Output (GPIO), Inter Integrated Circuit (I^{2}C) commands, and power supply over a single UTP cable, with a maximum distance of $15m$ between two nodes and a maximum total length of $40m$ for the entire A^{2}B network. The bus has a maximum bandwidth of $50Mbps$ allowing to transport up to 32 channels (32-bit word width) at a sample rate of $44.1kHz$ or $48kHz$. Up to 11 nodes (one main node and 10 subordinate nodes) can be connected in daisy-chain. A^{2}B technology keeps all the nodes synchronized with negligible jitter effect [29] on a sensors network [30], and offers a deterministic latency of about $50\mu s$ (2 samples time) between any node. Access to the bus is managed by dedicated transceivers, thus simplifying the design process of the nodes. Moreover, there is no need to develop complex software applications, since a simple microcontroller is sufficient, and it is required only for the initial configuration of the bus (start-up phase). A comprehensive description of A^{2}B bus and A^{2}B network can be found in [31].

Fig. 2 a) shows the block diagram of the proposed digital acquisition sub-node. Sensors are acquired by specifically designed subordinate boards, which offer different types of interfaces to accommodate commonly used industrial sensors. Each node can acquire up to four channels from Integrated Electronics Piezo-Electric (IEPE) sensors, voltage output sensors (the voltage range is from $-10V$ to $10V$), and digital sensors with Integrated Interchip Sound (I^{2}S) or Pulse Density Modulation (PDM) interface. Analog sensors (IEPE or with voltage output) are acquired by an ADC, which communicates with the A^{2}B transceiver through I^{2}S interface. When employing IEPE sensors, their excitation supply can be remotely enabled by means of the A^{2}B transceiver GPIO. Instead, when voltage output sensors are used, IEPE excitation will be disabled, and sensors will be power supplied by a dedicated voltage regulator. The subordinate board can be power supplied by the A^{2}B bus (up to $2.7W$ per bus) or by an external power supply. Finally, the board also has auxiliary lines, namely GPIO and I^{2}C, useful to connect with external devices (e.g., relays or limit switches) or acquire other kind of sensors (e.g., I^{2}C temperature sensors). Fig. 2 b) shows a 3D rendering of the full-digital sub-node prototype, integrating the tri-axial MEMS accelerometer. A coin was positioned next to the board for size comparison.

Channels are then routed to the A^{2}B main node, which comprises up to four A^{2}B main transceivers, all synchronized by the same clock source. Several main nodes can be linked together to further increase the total number of channels and so to extend the maximum distance covered by the sensors. The choice depends on the specific application: if many sensors are required at a short distance from each other, a single main node with three or four A^{2}B buses is preferable, otherwise more than one main node can be used, each one equipped with only one or two A^{2}B networks. In [32] and [33], three main nodes with two A^{2}B buses each one were used, for a total number of channels equal to 160 distributed along $20m$. The same clock of the A^{2}B network is shared also to digital MEMS accelerometers through Time-division Multiplexing

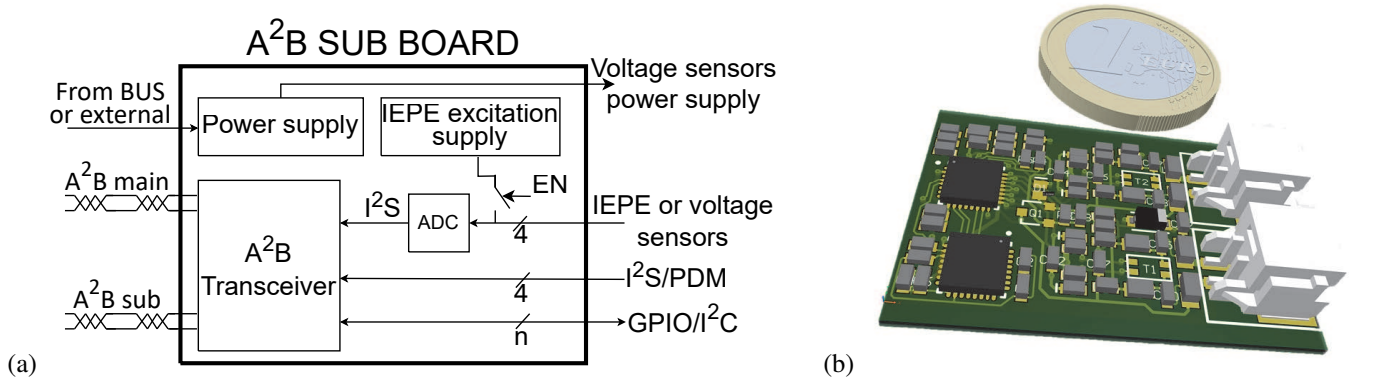

Fig. 2. Universal A^{2}B sub-node: a) Block diagram of the designed subordinate board compliant with voltage, IEPE and I^2S/PDM sensors. b) 3D rendering of the full-digital sub-node prototype with a coin for size comparison.

(TDM) signals, thus allowing to synchronously sample both digital and analog nodes. The clock propagation model of an A^{2}B network featuring ten nodes was developed and discussed in [29]. In particular, the jitter presents a predominant random component (RJ), whilst the deterministic component (DJ) can be neglected. The latency, on the contrary, is deterministic and its value is about $154ns$ for each sub-node, as shown by measures. However, latency can be compensated with a resolution of about $20ns$, using a specific A^{2}B protocol feature. Simulations of an array composed of 28 sensors have been carried out in [30], where the jitter effects have been made significant by increasing artificially the measured values by a factor 1000. Eventually, experimental results also confirmed that clock propagation effects can be neglected.

In addition, the main board must have a microcontroller that initializes the buses through an I^{2}C communication with the main transceivers. During the normal operation of the bus, the microcontroller may also check for faults and manage the I^{2}C and GPIO over A^{2}B. The last purpose of the main board is to convert A^{2}B to a protocol suitable for the acquisition from an industrial Personal Computer (PC), allowing at the same time to reach greater distances (A^{2}B is limited to $40m$), thus increasing the application range of the proposed acquisition system. Protocol conversion can be accomplished by a microcontroller, a processor, or a Field Programmable Gate Array (FPGA). Ethernet based protocols are commonly used in industrial applications [34], [35], but in this paper Universal Serial Bus (USB) was chosen. A single USB connection can handle all the 32 channels of a single A^{2}B bus operating at $48kHz$ with 32-bit word width.

Finally, it must be pointed out that the proposed acquisition system is highly scalable as it can be easily expanded not only by increasing the number of sensors or buses on an A^{2}B main board, but also by adding other main boards. Ethernet based protocols are particularly suitable for this purpose, since boards can be connected by means of switches and traffic can be routed to the PC on a single ethernet cable, as in Audio Video Bridging (AVB) [36] or Dante [37] systems.

In the present work, a single motor application has been investigated in order to demonstrate the effectiveness of the technology. However, the main advantages can be observed on a distributed system where many sensors are installed, such as large machinery or industrial production plants. The proposed DAQ system is particularly suitable also for SHM of civil structures and infrastructures [38]. Example of these possible applications are long bridges, high-rise structures, and large buildings. In these applications, the proposed system would provide a series of advantages with respect to traditional ones. Above all, ensuring accurate data synchronization, which is mandatory for modal analysis, considerably reduction of cabling length, system complexity, and overall cost. Eventually, even in-situ measurements can benefit from such a solution, as quick and easy installation is crucial for temporary applications.

The proposed architecture also shows a few disadvantages. Each analog node can handle up to four channels, which may result in a waste of resources when only a triaxial accelerometer or an inclinometer are connected to a single node, thus leaving one or two channels unused. The sampling frequency is fixed at $48kHz$, a suitable value for most industrial applications. However, in particular cases, such as structural civil monitoring or high-speed motor drives, it can be too high or too low, respectively.

IV. Hybrid DAQ System validation

The proposed hybrid A^{2}B DAQ system has been validated by comparing it against a commercial, laboratory grade, DAQ based on NI-9234 module. The comparison was carried out using the same piezoelectric mono-axial accelerometer (PCB 333B30), having a full-scale of $+/-50g$ and a sensitivity of $100mV/g$. Two kind of tests have been performed: a background noise measurement and a forced response test.

The first experiment was aimed at assessing the background noise: the sensor was mounted on a $1000kg$ inertial mass positioned in the Acoustics and Vibration laboratory at the Department of Engineering and Architecture (University of Parma), and recorded over the course of several nights (to minimize the presence of ambient vibrations) at the standard sampling frequency $fs = 48kHz$. A first set of measurements was obtained by connecting the accelerometer to the proposed DAQ system. As a term of comparison, a second set of measurements was obtained by connecting the accelerometer

to a commercial DAQ (NI-9234). The resulting spectra are compared in Fig. 4 in terms of Power Spectral Density (PSD). One can note that the PSD are almost identical below $60Hz$. As the lab is not an ElectroMagnetic Interference (EMI) neutral environment, instead with several electronic equipment switched on during the entire measurement, among the notable differences a better mains frequency ($50Hz$) rejection of the proposed DAQ is observed, related to a better filtered power supply stage and its intrinsic digital architecture. This immunity to mains frequency disturbances is particularly useful in industrial applications. The second notable difference is the average spectral noise above $60Hz$, that is about $6.5^{-7}m/s^2/\sqrt{H}z$ for the commercial DAQ system and a higher $1.6^{-6}m/s^2/\sqrt{H}z$ for the proposed hybrid DAQ solution. The higher average spectral noise is mainly due to the lower ADC resolution (16-bit for the proposed vs. 24-bit of the commercial DAQ).

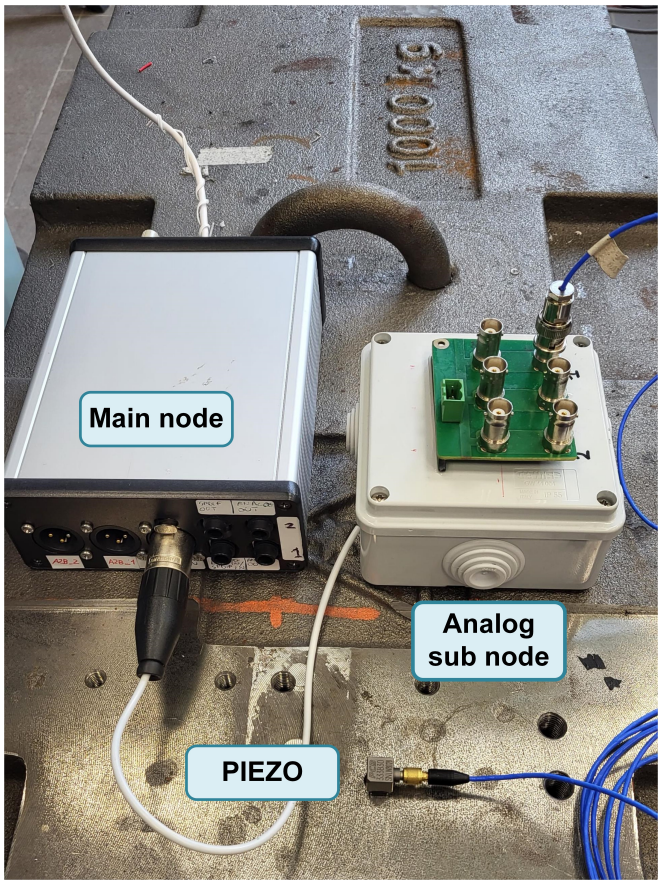

Fig. 3. Experimental setup for background noise measurement. Left: A^{2}B interface. Right: ADC sub-node. Below: piezoelectric accelerometer.

For the forced response test experiment, the same piezoelectric transducer was mounted on a modal shaker, Bruel&Kjaer (B&K) type 4810, excited with a special test signal, an Exponential Sine Sweep (ESS) covering a frequency range from $15Hz$ to $1kHz$, delivered through an analog amplifier. The amplifier was set at an output voltage of $1V$, which in turn makes the shaker to vibrate with an acceleration of $1m/s^2$, corresponding to $120dB$ re $a_{ref} = 10^{-6}m/s^2$.

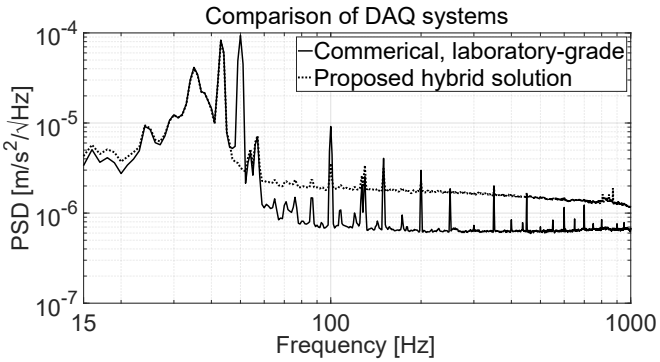

Fig. 4. Power Spectral Density of two DAQ systems.

The measurements were again performed twice, at first with the accelerometer connected to a commercial DAQ (NI-9234), then by connecting the piezoelectric accelerometer to the ADC sub-node of the proposed hybrid A^{2}B DAQ system, (Fig. 5). The recorded ESS were processed by means of the convolution with the associated inverse filter, specifically inverse-ESS, thus obtaining the time domain Impulse Responses (IRs) [39] of the system. The linear IRs was analyzed in frequency domain with the Fast Fourier Transform (FFT).

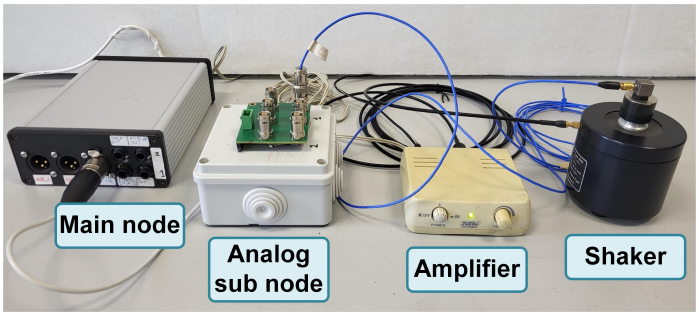

Fig. 5. Experimental setup for the measurement of accelerometer transfer functions. From left to right: 1) A^{2}B interface, 2) ADC sub-node, 3) Analog amplifier, 4) B&K modal shaker with accelerometer.

Fig. 6 shows the transfer functions (TF) of the two measurements in the frequency range $15Hz - 1kHz$. One can note they are identical in the entire frequency range. The TF is not flat, due to the limited response of the modal shaker: it exhibits a resonance at $50Hz$, which causes an overshoot of $5dB$, and a decreasing efficiency from $30Hz$ and below.

V. Case Study Experimental Measurements

The case study of bearing fault diagnosis via vibration signals was chosen for the experimental evaluation of the proposed DAQ system. Different rolling bearing fault scenarios were employed to experimentally assess the performance of the proposed vibration monitoring system. Radial bearings are widely used in every rotating machinery: they consist of two concentric rings with inner and outer races machined on them, separated by spherical or cylindrical rolling elements, Fig. 7. Rolling elements are usually kept equally spaced by a cage, thus allowing for even load distribution, and preventing rubbing during normal operation.

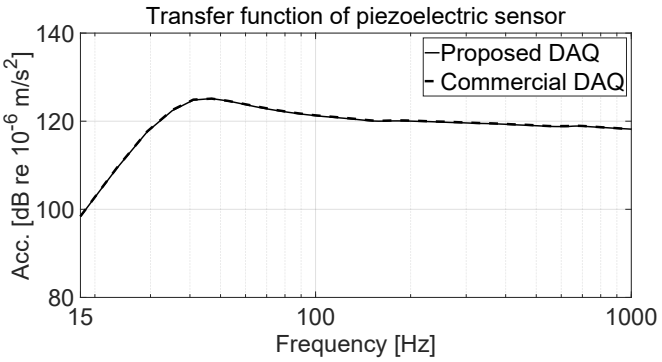

Fig. 6. Transfer functions of a piezolectric accelerometer measured with two DAQ systems.

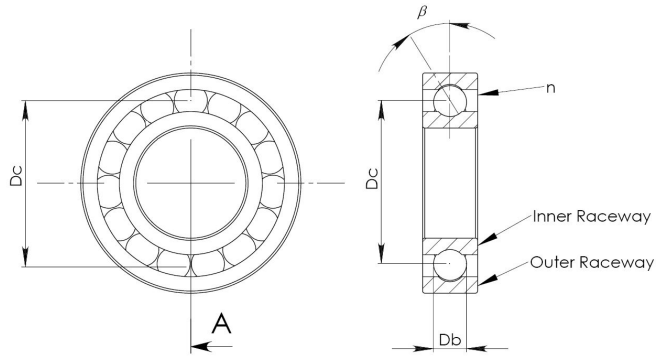

Fig. 7. Ball bearing structure, highlighting the characteristic dimensions. Cage is not depicted to simplify representation.

Faults localized on different components of the bearing produce different characteristic vibration frequency components, that can be considered signatures of that fault. These characteristic bearing fault frequencies depend on the bearing construction (i.e., the bearing geometry) and the relative speed of the outer and the inner ring. The following equations are obtained by considering the outer ring fixed to the frame, so that the characteristic mechanical vibration frequencies can be calculated from the bearing's physical dimensions, Fig. 7.

$$F_{cage} = \frac{1}{2} F_r \left(1 - \frac{D_b \cos\beta}{D_c}\right) \quad (1)$$

$$F_{outer} = \frac{n}{2} F_r \left(1 - \frac{D_b \cos\beta}{D_c}\right) \quad (2)$$

$$F_{inner} = \frac{n}{2} F_r \left(1 + \frac{D_b \cos\beta}{D_c}\right) \quad (3)$$

$$F_{ball} = \frac{D_c}{D_b} F_r \left[1 - \left(\frac{D_b \cos\beta}{D_c}\right)^2\right] \quad (4)$$

where n is the number of rolling elements (i.e., balls in the present work), D_b is the rolling element diameter, D_c is the pitch diameter, β is the ball contact angle, Fig.7. Table II reports the specifications of the bearing used in the experiments and Table III summarizes the corresponding signature frequencies when the machine is operated at no load, with a mechanical speed of 998 Revolutions per Minute (RPM) ($F_r = 16.3Hz$). The operating speed was measured with a Compact A2103/LSR laser tachometer.

TABLE II
SPECIFICATIONS OF THE BALL BEARING USED IN THE EXPERIMENTS

Inner diameter	25	$[mm]$
Outer diameter	52	$[mm]$
Number of spheres	9	
Basic static load rating	7800	$[N]$
F_{inner}/F_r	5.41	
F_{outer}/F_r	3.585	
F_{cage}/F_r	0.398	
F_{ball}/F_r	4.715	

TABLE III
EXPECTED FAULT FREQUENCIES OF THE BALL BEARING USED IN THE EXPERIMENTS

f	50	Hz
F_r	16.3	Hz
F_{inner}	88.2	Hz
F_{outer}	58.4	Hz
F_{cage}	6.5	Hz
F_{ball}	76.9	Hz

The following subsections are respectively dedicated to detail the data acquisition system characterization, the test setup, and reporting the obtained experimental results.

A. DAQ system characterization

The acquisition system employed for the experimental measurement features an A^{2}B main board and three A^{2}B subordinate boards. Two of the three subordinate nodes integrate a tri-axial MEMS accelerometer, having a full-scale value of $+/-16g$ and 14-bit digital output. A low-pass filter integrated in the MEMS transducers was enabled at $300Hz$, for improving the S/N. The third subordinate node integrates a 3-channels ADC, which allows acquiring a tri-axial piezoelectric accelerometer. Since the main excitation of the system was expected along the vertical axis, a mono-axial accelerometer was used, with a full-scale value of $+/-50g$ and a sensitivity of $100mV/g$. Similarly, only the Z-axis of the MEMS were recorded. A USB connection was employed between the host PC and the main A^{2}B board. At first, the accelerometers have been calibrated, with a B&K calibration system type 4294. It produces a pure tone at $159.2Hz$ with an acceleration of $a_{cal} = 10m/s^2$ ($140dB$ re $a_{ref} = 10^{-6}m/s^2$). A signal of $20s$ was recorded for each accelerometer, and the full-scale values have been calculated as:

$$FS = 20 * log10(\frac{a_{cal}}{a_{ref}}) - 20 * log10(a_{rms}) \quad (5)$$

where a_{cal} is the calibration value, a_{ref} is the reference value for deciBel conversion, and a_{rms} is the RMS value of the recorded acceleration signal. Results are summarized in Table IV.

Then, the accelerometer TFs were measured with a modal shaker, with a similar procedure described in section III, see Fig. 5. Fig. 8. shows the superimposed spectra for the three

TABLE IV
FULL-SCALE VALUE OF PIEZOELECTRIC AND MEMS ACCELEROMETERS

Transducer	FS Value
Piezoelectric	169.1 dB
MEMS 1	165.7 dB
MEMS 2	165.3 dB

different accelerometers, in the frequency range $15Hz-1kHz$. An excellent superimposition of the TF is observed in the range $30Hz-300Hz$, within $+/-0.5dB$. It is also possible to note that the frequency response of MEMS accelerometers starts to roll off above $300Hz$, which is the cutoff frequency of the internal filter. At the calibration frequency, that is $159.2Hz$, the three spectra coincide at $120dB$, corresponding to $1m/s^2$.

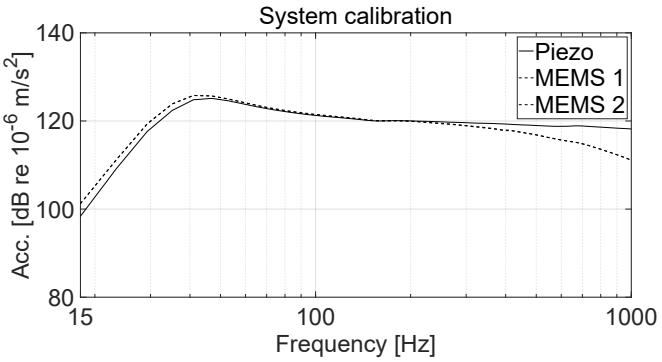

Fig. 8. Accelerometer transfer functions.

B. Test setup

The experimental test run for bearing fault diagnosis via vibration signals were carried out by interfacing the proposed data acquisition system to a motor test bench. Both MEMS as well as piezoelectric transducers were employed in order to assess their respective performance and to demonstrate the flexibility in the configuration of the proposed data acquisition system. The test bench, Fig. 9, is constituted of a welded steel rigid frame that houses the motor under test (MUT) and the transducer network to acquire vibration signals. The MUT employed during the tests is a 6 poles induction machine, that is directly connected to the $400V50Hz$ three-phase mains grid. Table V summarizes the relevant nameplate data of the MUT.

TABLE V
NAMEPLATE DATA OF THE MOTOR UNDER TEST

Specification	Value
Nominal Power	1100 W
Number of poles	6
Nominal current	2.8 A
Power Factor	0.76
Nominal Torque	11.5 Nm (8.5 $FtLbs$)
Stator Resistance	5.65 Ω

At first, a reference measurement was taken on a bearing without any defects. Then the drive end bearing was replaced

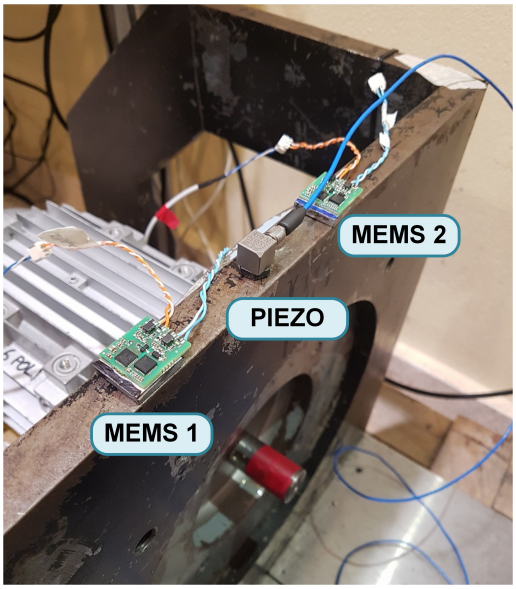

Fig. 9. Test setup overview, showing the IEPE piezoelectric transducer (center) flanked by the MEMS modules, installed on the steel frame holding the motor under test.

with an artificially damaged one. For the motor bearing condition monitoring scenario, two test bearings were employed, each with different damages. Both fault cases scenarios represents realistic damages due to wear or errors in assembly and were already presented in literature [40]. They are obtained in the laboratory by altering healthy bearings:

- One bearing featured a single defect on the outer race. The defect was created by chemical etching of the bearing outer raceway, Fig. 10-left. This type of fault reproduces a localized fault with only a characteristic signature at F_{outer}, Eq. (2).
- On another bearing, a simulated brinelling fault was reproduced by a concentrated mechanical overload of $4tons(40kN)$ to the bearing, Fig. 10-right. This type of fault involves all the three major components of the bearing with the sole exception of the cage. The test aims at reproducing a more realistic fault, characterized by the simultaneous presence of multiple fault characteristic vibration components at F_{outer}, F_{inner} and F_{ball}).

C. Results

At first, the measurement of the healthy bearing was analyzed, by calculating the amplitude spectra for the piezoelectric and the MEMS transducers, shown in Fig. 11. The spectra were calculated making use of the FFT algorithm, with a frequency resolution given by:

$$df = \frac{fs}{n_{FFT}} \tag{6}$$

where $fs = 48kHz$ is the sampling frequency of the A^2B bus and $n_{FFT} = 2^{16}$ is the number of frequency bins employed. Only the vertical axes of the MEMS were considered, for being comparable with the piezoelectric accelerometer.

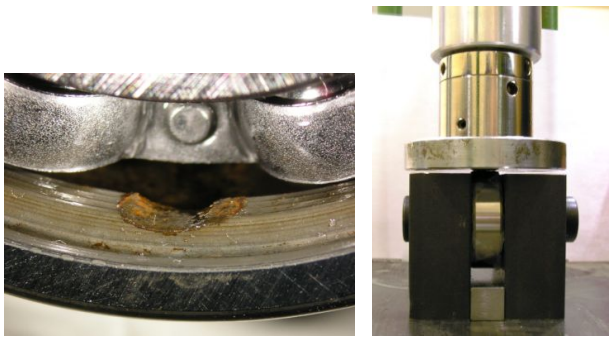

Fig. 10. Microphotography of the chemically etched outer race single defect (left). Photo of the hydraulic press employed to impart bearing brinelling damage (right).

One can note that the supply frequency component $f = 50Hz$, can be seen only on the piezoelectric transducer, as it is captured by the analog stage. On the other hand, the supply frequency 2^{nd} harmonic $2f = 100Hz$ is present in the spectra of all the three transducers. The vibration frequency at twice electrical line frequency is inherent for all alternate current electrical machinery vibration spectra as a result of a machine structure's excitation under the action of variable electromagnetic forces. Other two peaks are observed, corresponding to the mechanical speed of the MUT, F_r and $2F_r$, as the result of a slight mechanical imbalance. From the comparison of the spectra, it is also possible to note that the noise floor of the MEMS transducers ($2 * 10^{-2} m/s^2$) is higher than the piezoelectric one ($10^{-3} m/s^2$). Despite this, both types of transducers allowed identifying correctly the main information of the system under investigation. Charts start from $16Hz$, since defects do not involve any damage on the cage, and so the minimum frequency of interest coincides with the rotation frequency, F_r.

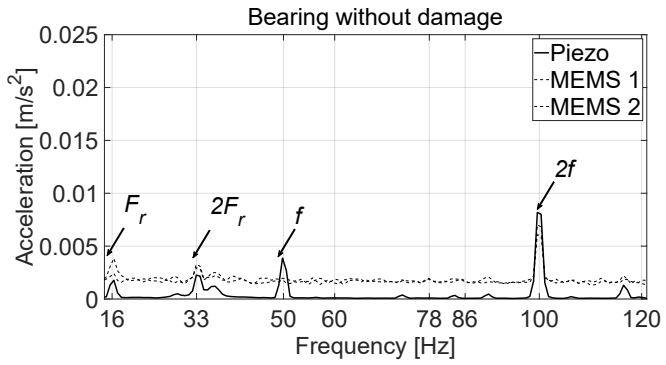

Fig. 11. Amplitude spectra of the three accelerometers for a not damaged bearing.

Then, the amplitude spectra for the piezoelectric and the MEMS transducers were calculated also for damaged bearings. Fig. 12 shows the result for the single defect on the outer race of the bearing (Fig. 10-left). The previously observed peaks are still present. In addition, the peaks at F_{outer} and at $2F_{outer}$ are clearly discernible in the spectra of both type of transducers.

Fig. 13 shows the results for the simulated brinelling fault,

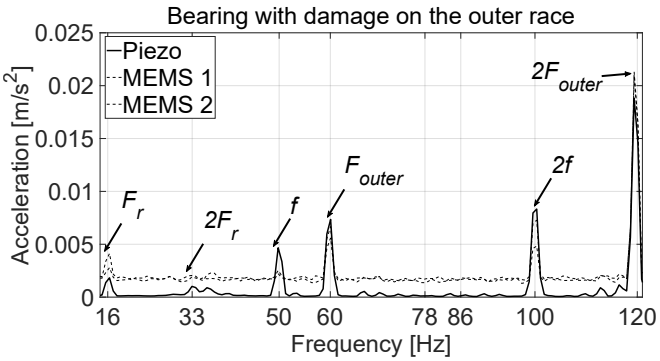

Fig. 12. Amplitude spectra of the three accelerometers for a bearing with outer race damage.

which causes several fault characteristic frequencies to appear at the same time, as described by Eq. 2 - 4. In particular, as a notable difference with the previous single defect case, the spectra now exhibit a peak at F_{ball} and at F_{inner} frequencies as well.

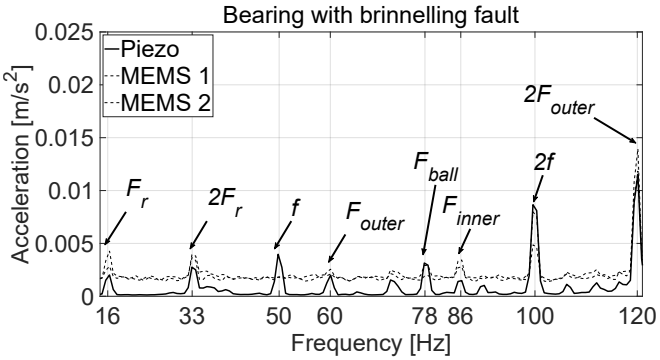

Fig. 13. Amplitude spectra of the three accelerometers for a bearing with a simulated brinelling damage.

To further assess the accuracy of the system when different transducers (analogue and digital) are employed in the same sensor network, the TFs between each MEMS and the piezoelectric accelerometer have been calculated. Fig. 14 shows the result for the first case, hence a healthy bearing. It is worth noticing that at those frequencies where the signal, and so the S/N, is high, the magnitude of the TFs is equal to 1 and the phase is equal to $0rad$. These conditions mean that the measurements from piezoelectric and the MEMS transducers are providing exactly the same information.

Fig. 15 and Fig. 16 show the TFs for the cases of damage on the outer race and simulated brinelling fault, respectively. Being the excitation stronger due to the presence of a damage, a greater similarity between the two types of transducer is observed in both cases.

VI. Discussion

The performance of the proposed DAQ system was experimentally assessed by a number of different tests. In the first experiment, the hybrid sensor node of the proposed DAQ system has been validated by comparison against a commercial, laboratory grade setup. Characterization was carried out both

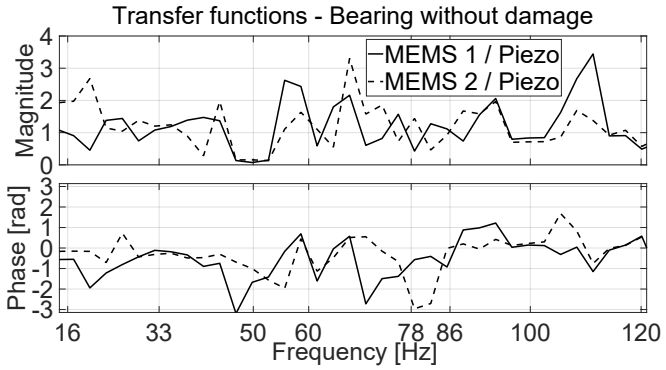

Fig. 14. Transfer function between MEMS and piezoelectric accelerometers for a bearing without damage.

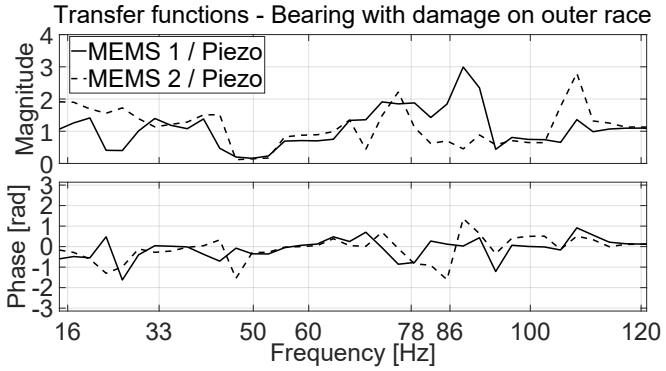

Fig. 15. Transfer function between MEMS and piezoelectric accelerometers for a bearing with an outer race damage.

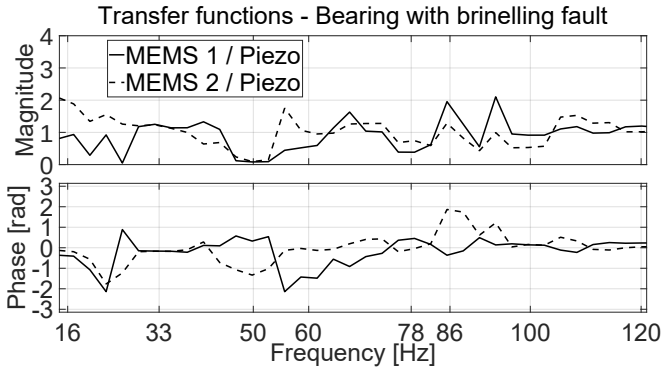

Fig. 16. Transfer function between MEMS and piezoelectric accelerometers for a bearing with a simulated brinelling damage.

in terms of background noise measurement, with the sensor mounted on a $1000kg$ inertial mass, and with a forced response on a modal shaker. The proposed DAQ system exhibited a response perfectly overlapping the one of the commercial system, and in case of the background noise, the proposed solution demonstrated a higher immunity to the $50Hz$ mains electrical noise, Fig. 4.

A second, expected, outcome of the comparison was the average spectral noise above $60Hz$, where the commercial system performed better, mainly due to the lower ADC resolution of the proposed DAQ (16-bit vs. 24-bit of the commercial DAQ). The results of the forced response test in the frequency range $15Hz - 1kHz$ confirmed again a perfectly overlapping response with the commercial system, Fig. 6

The proposed DAQ system capability to operate with different transducers in a hybrid configuration was then demonstrated in the second set of experiments. An A^{2}B DAQ setup consisting of three subordinate nodes was prepared, two nodes were fitted with a tri-axial MEMS accelerometer, $(+/-16g$, 14-bit digital output and $300Hz$ integrated low-pass filter) and the third one featured a 3-channels ADC to interface with piezoelectric transducers. The hybrid configuration DAQ system was first calibrated on a modal shaker, with a procedure similar to the one described in section III. The spectra for the three different accelerometers showed excellent superimposition within $+/-0.5dB$ of the TFs in the range $30Hz-300Hz$, Fig. 8. As expected, MEMS obtained TF shown a roll-off past $300Hz$ due to the internal low-pass filter.

The hybrid configuration DAQ system was then employed to detect vibration fault signatures in the scenario of motor bearing condition monitoring. Different rolling bearing fault cases were employed to experimentally assess the performance of the proposed vibration monitoring system: one bearing featured a single defect on the outer race, the other exhibited a simulated brinelling fault. In all the cases, when analyzing the vibration spectra, fault signatures of the specific damages were clearly discernible in the spectra of both type of transducers (MEMS and piezoelectric). Fig. 12 refers to the single defect on the outer race, showing the F_{outer} component, and Fig. 13 refers to brinelling fault, with F_{outer}, F_{ball} and at F_{inner} components appearing together at the same time. The main notable difference from the comparison of the spectra in the hybrid configuration, was that the noise floor of the MEMS transducers $(2 * 10^{-2} m/s^2)$ is higher than the piezoelectric one $(10^{-3} m/s^2)$. Apart form that, the measurements from piezoelectric and the MEMS transducers provided exactly the same information, as it was also testified by computing the TF between each MEMS and the piezoelectric accelerometer, shown in Fig. 14.

VII. Conclusion

This paper presents a novel DAQ system particularly suited to manage large sensor arrays for vibration-based condition monitoring on complex machinery. The proposed system features minimal latency and excellent bandwidth. The proposed solution aims at filling a gap between the centralized DAQ platforms and the networked vibration sensor nodes, by providing a 16-bit resolution (24-bit nodes are being developed) digital DAQ network characterized by a fast 48 kHz sampling frequency. The proposed solution is based on A^{2}B digital bus, which allows for connecting several acquisition nodes on a daisy-chain topology. Together with the use of an UTP wire, this solution provides a considerably reduction of the overall length/mass and cost of the cabling, especially when compared against traditional centralized solutions requiring coaxial cables to connect to the transducers. In addition, A^{2}B bus grants data integrity also in electromagnetic polluted environments. It also grants perfect temporal alignment of the different channels: the resulting data synchronization is

mandatory for modal analysis and time domain correlation between signals coming from different acquisition boards or different positions of large machinery.

A hybrid acquisition node has been designed, integrating an Analog-to-Digital conversion for acquiring standard piezoelectric transducers. This entails a significant increase in the flexibility of the system without compromising its simplicity. In fact, the co-existence of low-cost MEMS together with top-quality piezoelectric transducers, allows for optimizing the performance and the cost of the sensor network. Since A^2B delivers also phantom power supply on the same UTP cable, no additional wires are required for providing power supply to piezoelectric transducers.

The main advantages of the proposed solution are: scalability, ease of reconfiguration, flexibility of transducers choices, and fully digital two-wire bus connection that simplify wiring on the field and guarantees negligible jitter and delay between samples.

The effectiveness of the proposed solution was proved with an experimental test. A 6-poles induction machine was measured with three different types of ball bearing: a healthy bearing without any damage and two bearings with simulated faults, one with a single defect on the outer rage and one with a brinelling fault. A sensor network comprising three acquisition nodes was employed, of which two full-digital, integrating tri-axial MEMS accelerometers, and one hybrid to acquire a piezoelectric accelerometer. The spectra and the transfer functions have been compared in the frequency range $16Hz - 120Hz$, showing an excellent agreement between the analog and the digital information, despite a significant difference in the cost and quality of the sensors. It has been possible to identify both artificial defects, as well as the healthy bearing, and the mechanical characteristic of the system, such as the angular frequency.

REFERENCES

[1] A. Garcia-Perez, R. d. J. Romero-Troncoso, E. Cabal-Yepez, and R. A. Osornio-Rios, "The application of high-resolution spectral analysis for identifying multiple combined faults in induction motors," *IEEE Transactions on Industrial Electronics*, vol. 58, no. 5, pp. 2002–2010, 5 2011, doi: 10.1109/TIE.2010.2051398.

[2] A. H. Bonnett, "Root cause ac motor failure analysis with a focus on shaft failures," *IEEE Transactions on Industry Applications*, vol. 36, no. 5, pp. 1435–1448, 9 2000, doi: 10.1109/28.871294.

[3] ABB Ltd. (2015, consulted 2022-12-09) A guide to preventing failure. [Online]. Available: https://new.abb.com/docs/librariesprovider53/about-downloads/motors_ebook.pdf

[4] G. Curcuru, M. Cocconcelli, F. Immovilli, and R. Rubini, "On the detection of distributed roughness on ball bearings via stator current energy: Experimental results," *Diagnostyka*, vol. 51, no. 3, pp. 17–21, 2009.

[5] L. Frosini and E. Bassi, "Stator current and motor efficiency as indicators for different types of bearing faults in induction motors," *IEEE Transactions on Industrial Electronics*, vol. 57, no. 1, pp. 244–251, 1 2010, doi: 10.1109/TIE.2009.2026770.

[6] J. R. Stack, T. G. Habetler, and R. G. Harley, "Fault-signature modeling and detection of inner-race bearing faults," *IEEE Transactions on Industry Applications*, vol. 42, no. 1, pp. 61–68, 1 2006, doi: 10.1109/TIA.2005.861365.

[7] S. Choi, B. Akin, M. M. Rahimian, and H. A. Toliyat, "Performance-oriented electric motors diagnostics in modern energy conversion systems," *IEEE Transactions on Industrial Electronics*, vol. 59, no. 2, pp. 1266–1277, 2 2012, doi: 10.1109/TIE.2011.2158037.

[8] *ISO 10816-1: Evaluation of machine vibration by measurements on non-rotating parts*. Interstate Council For Standardization, Metrology And Certification Std.

[9] R. B. Randall, *Vibration based condition monitoring*. Wiley and sons, 2011.

[10] J. Yu, "Local and nonlocal preserving projection for bearing defect classification and performance assessment," *IEEE Transactions on Industrial Electronics*, vol. 59, no. 5, pp. 2363–2376, 5 2012, doi: 10.1109/TIE.2011.2167893.

[11] D. C. Mazur, J. A. Kay, and K. D. Mazur, "Advancements in vibration monitoring for the mining industry," *IEEE Transactions on Industry Applications*, vol. 51, no. 5, pp. 4321–4328, 2015, doi: 10.1109/TIA.2015.2416151.

[12] C. R. Farrar and K. Worden, *An Introduction to Structural Health Monitoring*. Springer Vienna, 2010, pp. 1–17, doi: 10.1007/978-3-7091-0399-9_1.

[13] C. Farrar and K. Worden, *Structural Health Monitoring A Machine Learning Perspective*. Wiley, 1 2013.

[14] F. Luca, S. Manzoni, A. Cigada, and L. Frate, "A vibration-based approach for health monitoring of tie-rods under uncertain environmental conditions," *Mechanical Systems and Signal Processing*, vol. 167, p. 108547, 2022. [Online]. Available: https://www.sciencedirect.com/science/article/pii/S0888327021008876

[15] M. Masciotta, A. Barontini, L. Ramos, P. Mendes, and P. Lourenco, "An overview on structural health monitoring: From the current state-of-the-art to new bio-inspired sensing paradigms," *International Journal of Bio-Inspired Computation*, 9 2018.

[16] A. Abdaoui, T. El-Fouly, and M. Ahmed, "Impact of time synchronization error on the mode-shape identification and damage detection/localization in wsns for structural health monitoring," *Journal of Network and Computer Applications*, vol. 83, pp. 181–189, 4 2017.

[17] M. Haque, "Transmission loss computed of star topology sensor network base on dt, red and sfq buffer mechanism for overseeing high rise building structural health," *International Journal of Bioscience, Biochemistry and Bioinformatics*, vol. 3, pp. 646–649, 01 2013.

[18] T.-H. Wu, C.-Y. Sue, and P.-Y. Chen, "Intelligent data acquisition system for mems vibration monitoring applications," in *2018 13th International Microsystems, Packaging, Assembly and Circuits Technology Conference (IMPACT)*, 2018, pp. 252–255, doi: 10.1109/IMPACT.2018.8625743.

[19] G. Weiming, Z. Ming, G. Xinfeng, D. Yongsheng, D. Jinqi, and Z. Yizhong, "Vibration data acquisition and fault diagnosis system of hydro turbine based on compactrio," in *2017 5th International Conference on Mechanical, Automotive and Materials Engineering (CMAME)*, 2017, pp. 319–323, doi: 10.1109/CMAME.2017.8540176.

[20] L. Zhao, Y. Zhou, I. B. M. Matsuo, S. K. Korkua, and W.-J. Lee, "The design of a remote online holistic monitoring system for a wind turbine," *IEEE Transactions on Industry Applications*, vol. 56, no. 1, pp. 14–21, 2020, doi: 10.1109/TIA.2019.2951088.

[21] S. Gao, X. Zhang, C. Du, and Q. Ji, "A multichannel low-power wide-area network with high-accuracy synchronization ability for machine vibration monitoring," *IEEE Internet of Things Journal*, vol. 6, no. 3, pp. 5040–5047, 2019, doi: 10.1109/JIOT.2019.2895158.

[22] P. Jiao, K.-J. I. Egbe, Y. Xie, A. Matin Nazar, and A. H. Alavi, "Piezoelectric sensing techniques in structural health monitoring: A state-of-the-art review," *Sensors*, vol. 20, no. 13, 2020. [Online]. Available: https://www.mdpi.com/1424-8220/20/13/3730

[23] M. B. Moffett and J. M. Powers, "Noise in piezoelectric sensors," *The Journal of the Acoustical Society of America*, vol. 88, no. S1, pp. S160–S160, 1990.

[24] M. Varanis, A. Silva, A. Mereles, and R. Pederiva, "Mems accelerometers for mechanical vibrations analysis: a comprehensive review with applications," *Journal of the Brazilian Society of Mechanical Sciences and Engineering*, vol. 40, 2018.

[25] S. Thanagasundram and F. Schlindwein, "Comparison of integrated micro-electrical-mechanical system and piezoelectric accelerometers for machine condition monitoring," *Proceedings of the Institution of Mechanical Engineers Part C Journal of Mechanical Engineering Science 1989-1996 (vols 203-210)*, vol. 220, pp. 1135–1146, 04 2006.

[26] S. Kavitha and K. Joseph Daniel, R. Sumangala, "High performance mems accelerometers for concrete shm applications and comparison with cots accelerometers," *Mechanical Systems and Signal Processing*, vol. 66-67, pp. 410–424, 2016. [Online]. Available: https://www.sciencedirect.com/science/article/pii/S0888327015002915

[27] K. Waurin, "Innovative digital bus architecture reduces audio system costs," Norwood, MA, USA, 2018. [Online]. Available: https://www.analog.com/media/en/technical-documentation/tech-articles/Innovative-Digital-Bus-Architecture-Reduces-Audio-System-Costs.pdf

[28] J. Triggs, "The a to z of a2b applications," Norwood, MA, USA, pp. 1–4, 9 2020. [Online]. Available: https://www.analog.com/en/analog-dialogue/articles/the-a-to-z-of-a2b-applications.html
[29] N. Rocchi, A. Toscani, G. Chiorboli, D. Pinardi, M. Binelli, and A. Farina, "Transducer arrays over a^2b networks in industrial and automotive applications: Clock propagation measurements," *IEEE Access*, vol. 9, pp. 118 232–118 241, 2021, doi: 10.1109/ACCESS.2021.3106710.
[30] D. Pinardi, N. Rocchi, A. Toscani, M. Binelli, G. Chiorboli, A. Farina, and L. Cattani, "An innovative architecture of full-digital microphone arrays over a^2b network for consumer electronics," *IEEE Transactions on Consumer Electronics*, vol. 68, no. 3, pp. 200–208, 2022, doi: 10.1109/TCE.2022.3187453.
[31] N. Rocchi, A. Toscani, D. Pinardi, M. Binelli, L. Chiesi, A. Farina, E. Bonomi, and L. Tronchin, "A modular, low latency, a^2b-based architecture for distributed multichannel full-digital audio systems," in *2021 Immersive and 3D Audio: from Architecture to Automotive (I3DA)*, 2021, pp. 1–8, doi: 10.1109/I3DA48870.2021.9610947.
[32] A. Bevilacqua, L. Tronchin, M. Binelli, L. Chiesi, N. Rocchi, D. Pinardi, A. Toscani, and A. Farina, "Application of a wave field synthesis (wfs) audio system based on a^2b protocol: a case study," in *PROCEEDINGS of the 2nd Symposium: The Acoustics of Ancient Theatres*, 7 2022. [Online]. Available: http://www.angelofarina.it/Public/Papers/321-AIA-Verona-2022-3.pdf
[33] ——, "Design of a multichannel audio system based on a^2b architecture," in *PROCEEDINGS of the 2nd Symposium: The Acoustics of Ancient Theatres*, 7 2022. [Online]. Available: http://www.angelofarina.it/Public/Papers/320-AIA-Verona-2022-2.pdf
[34] J. Rinaldi, "Ethernet-ip - an application layer protocol for industrial automation," pp. 43–45, 5 2003. [Online]. Available: https://www.rtautomation.com/ethernet-ip-an-application-layer-for-industrial-automation/
[35] A. Baratella Lugli, J. Eduardo Moreira Souza, L. de Oliveira Pessoa, R. Lucano Ribeiro Rodrigues, and T. Henrique Moreno Tarifa, "Industrial ethernet networks and applications," *International Journal of Innovative Computing, Information and Control (IJICIC)*, vol. 12, no. 5, pp. 1505–1522, 10 2016, doi: 10.24507/ijicic.12.05.1505.
[36] J. Imtiaz, J. Jasperneite, and L. Han, "A performance study of ethernet audio video bridging (avb) for industrial real-time communication," in *2009 IEEE Conference on Emerging Technologies & Factory Automation*, 2009, pp. 1–8, doi: 10.1109/ETFA.2009.5347126.
[37] M. Pezzoli, L. Comanducci, J. Waltz, A. Agnello, L. Bondi, A. Canclini, and A. Sarti, "A dante powered modular microphone array system," *Journal of the Audio Engineering Society*, 10 2018, doi: .
[38] A. Toscani, N. Rocchi, D. Pinardi, M. Binelli, L. Saccenti, A. Farina, S. Pavoni, and M. Vanali, "Low-cost structural health monitoring system for smart buildings," in *2022 Second International Conference on Sustainable Mobility Applications, Renewables and Technology (SMART)*, 2022, pp. 1–7, doi: 10.1109/SMART55236.2022.9990379.
[39] A. Farina, "Simultaneous measurement of impulse response and distortion with a swept-sine technique," *Journal of the Audio Engineering Society*, 2 2000.
[40] F. Immovilli and M. Cocconcelli, "Experimental investigation of shaft radial load effect on bearing fault signatures detection," *IEEE Transactions on Industry Applications*, vol. 53, no. 3, pp. 2721–2729, 2017, doi: 10.1109/TIA.2016.2633236.

Andrea Toscani received the M.S. degree (cum laude) in electronic engineering and the Ph.D. degree in Information Technology from the University of Parma, Italy, in 2004 and 2008, respectively. His research activity is mainly focused on power electronics, high-performance electric drives, diagnostic techniques for industrial electric systems, and power converter for audio application. Since 2004, he has been working with the Department of Information Engineering (now, the Department of Engineering and Architecture), University of Parma, where he is currently a Research Fellow. Dr. Toscani is author of two patents.

Fabio Immovilli (S'08-M'11-SM'19) received the M.S. degree and the Ph.D. in Mechatronic Engineering at the University of Modena and Reggio Emilia, Italy, in 2006 and 2011 respectively. Since November 2019 he is an Associate Professor of Electric Converters, Machines and Drives at the Department of Sciences and Methods for Engineering, University of Modena and Reggio Emilia, Italy. He is the author or coauthor of more than 60 technical papers. His research interests include electric machine condition monitoring, electric power converters, machines for energy conversion from renewable energy sources, and thermoacoustics.

Daniel Pinardi received the M.S. degree (cum laude) in Mechanical Engineering from the University of Parma, Italy, in July 2016, with a thesis on loudspeaker modeling, and the Ph.D. in Industrial Engineering from the University of Parma, Italy, in March 2020, with a thesis on the design of microphone, hydrophone, and camera arrays for spatial audio recording. He has been a Research Assistant of Prof. Angelo Farina at University of Parma since 2016, mainly specialized in spatial audio, design of transducer arrays, acoustics simulations and 3D auralization, applied to automotive field, and underwater acoustics.

Luca Cattani received the Ph.D. degree in Information Technologies from the University of Parma, Italy, in 2016. His research interests include Advanced Signal Processing (Audio and Radio Frequency) for automotive applications. He is currently a Project Leader in the R&D department of ASK Industries SpA.